Journal of Chromatography A 1734 (2024) 465268

Contents lists available at ScienceDirect

Journal of Chromatography A

journal homepage: www.elsevier.com/locate/chroma

Fabrication of electrospun ion exchanger adsorbents with morphologies designed for the separation of proteins and plasmid DNA

Gyorgy Ovari [a,*], Thomas F. Johnson [a], Farzad Foroutan [b], Gunnar Malmquist [c], Matthew Townsend [b], Daniel G. Bracewell [a]

[a] Department of Biochemical Engineering, University College London, Gower Street, London WC1E 6BT UK
[b] Cytiva, Sycamore House, Gunnels Wood Road, Stevenage, SG1 2BP UK
[c] Cytiva Sweden AB, SE-751 84 Uppsala, Sweden

ARTICLE INFO

Keywords:
Electrospun adsorbents
Electrospinning
Protein adsorption
Plasmid DNA adsorption
X-ray computed tomography
BET surface area

ABSTRACT

Electrospun cellulose adsorbents are an emergent class of materials applied to a variety of bioprocess separations as an analogue to conventional packed bed chromatography. Electrospun adsorbents have proven to be effective as rapid cycling media, enabling high throughput separation of proteins and viral vectors without compromising selectivity and recovery. However, there is a current lack of knowledge in relation to the manipulation and control of electrospun adsorbent structure with function and performance to cater to the separation needs of emerging, diverse biological products.

In this study, a series of electrospun cellulose adsorbents were fabricated by adjusting their manufacturing conditions. A range of fiber diameters (400 to 600 nm) was created by changing the electrospinning polymer solution. Additionally, a range of porosities (0.4 to 0.7 v/v) was achieved by varying the laminating pressures on the electrospun sheets. The adsorbents were functionalized with different degrees of quaternary amine ligand density to create 18 prototype anion exchangers. Their morphology was characterized by BET nitrogen adsorption surface area, X-ray computed tomography, capillary flow porometry and scanning electron microscopy measurements.

The physical characteristics of the adsorbents were used in an adapted semi-empirical model and compared to measured permeability data. Permeabilities of prototypes ranged from 10^{-2} to 10^{-4} mDarcy. The measured data showed good adherence to modelled data with possible improvements in acquiring wet adsorbent characteristics instead of dried material. Finally, the electrospun adsorbents were characterized for their binding capacity of model proteins of different sizes (diameters of 3.5 nm and 8.9 nm) and plasmid DNA. Static binding capacities ranged from 5 mg/ml to 25 mg/ml for the proteins and plasmid DNA and showed <20 % deviation from monolayer coverage based on BET surface area. Therefore, it was concluded that the electrospun adsorbents most likely adsorb monolayers of proteins and plasmid DNA on the surface with minimal steric hindrance.

1. Introduction

Beaded packed-bed chromatography continues to serve as the primary unit operation for separation of biologics in the biotechnology and pharmaceutical sector. However, the industry has seen the emergence of novel biologic therapeutics, such as nucleic acids and viral vectors, which have unique separation challenges [1]. In order to overcome these challenges, new groups of chromatographic media have appeared both in industry and academia. Membranes, monoliths, and electrospun adsorbents are examples of chromatography media to facilitate the purification of novel biologics with products launched by many of the major manufactures [2–4]. Cited advantages of using novel chromatography media range from low mass transfer limitation, lower shear rates on particles, and reduced steric exclusion of larger biological products [5]. These quoted advantages can potentially lead to improved recoveries, process intensification and reduced cost of goods in downstream processing [1].

Electrospun adsorbents belong to a class of materials characterized by an internal structure of sub-micron-sized fibers [6]. The most widely adopted method to fabricate sub-micron-sized fibers is electrospinning,

* Corresponding author.
E-mail address: gyorgy.ovari.20@ucl.ac.uk (G. Ovari).

https://doi.org/10.1016/j.chroma.2024.465268
Received 23 May 2024; Received in revised form 24 July 2024; Accepted 13 August 2024
Available online 17 August 2024
0021-9673/© 2024 The Authors. Published by Elsevier B.V. This is an open access article under the CC BY license (http://creativecommons.org/licenses/by/4.0/).

involving the application of high voltage to a polymer solution [7,8]. The resultant high surface-area-to-volume ratio fiber structures have found applications in a wide range of areas, including fabrics, drug delivery, tissue engineering [9–12], and as solid adsorbents in liquid separations [13,14]. Among of electrospun adsorbents, cellulose is an ideal choice due to being extensively researched, widely available, and can be sourced sustainably [15]. To further improve electrospun adsorbent performance, the process of lamination can be utilised. Lamination has been shown to give mechanical strength and more controlled structures to the fibrous adsorbents [16,17]. Final stages of fabrication involve surface chemistry to deposit a functional ligand on the cellulose fibers to gain adsorptive properties.

The initial applications of cellulose electrospun adsorbents in bioprocessing were demonstrated in proof-of-concept papers utilizing model proteins in separations [18,19]. In Ma and Ramakrishna's study [18], electrospun adsorbents were functionalised with Protein A and Protein G, and placed in a centrifugal spin column devices to separate a mixture of BSA and monoclonal antibodies. At a similar time, Zhang et al. [19]. published on weak anion exchanger functionalised electrospun cellulose adsorbents that have higher static and dynamic binding capacities than then commercially available membranes.

The early studies on electrospun adsorbents showcased the feasibility of using electrospun adsorbents in bioprocessing. Furthermore, Hardick et al. [20]. demonstrated their competitive advantage in their ability to complete bind and elute cycles at flowrates over ten times higher than conventional beaded packed-bed media. This means that electrospun adsorbents have significantly higher productivity, enabling the rapid bind-and-elute cycling on large volumes of feed. This feature can be best exploited in capture steps where there is a need to process large volumes. Given this advantage, a highly productive electrospun adsorbent could be fully exhausted in a single batch, leading to the potential of single-use resins in a batch-to-batch setting [21]. This enables a more intensified process, fully single-use consumables and offers the potential for a more modular plant design [22,23]. In pursuit of these goals, later stages of development of electrospun adsorbent improved performance through lamination, showcased different ligand surface chemistries, and highlighted the possibility of adoption in continuous process chromatography [16,24]. Rajesh et al. focused on anion exchanged cellulose-based electrospun adsorbent with polyacrylonitrile grafts for protein adsorption while also studying model particle rejection [25]. In this study, electrospun adsorbents were studied for BSA adsorption for both static and dynamic capacities with values of 40 to 70 mg g^{-1} of adsorbent and observing an increased binding capacities at higher polymer grafting levels. A swelling of the fiber diameter was observed from the polymer grafts on the electron microscope images. Furthermore, adsorbents were shown to effectively retain dyed polystyrene microspheres above 100 nm. However, the investigation also does not connect these changes in physical structure (e.g. pore size and fiber diameter) to increased binding capacity and particle rejection.

The next generation of applications of electrospun chromatography resins can be classified into affinity and ion-exchange functionalisation. Firstly, in affinity capture of monoclonal antibodies using protein A, both membrane and electrospun adsorbents have seen comparable recoveries and host cell protein clearance as compared with packed-bed resins [26]. Adopting electrospun adsorbents in the capture step led to significant increases in volumetric productivity through rapid bind-and-elute cycling of large feed volumes [26,27].

Multiple studies have also investigated mRNA and viral vector capture using affinity ligands to take advantage of the reduced steric exclusion of larger biologics. Most recently, a study has shown that electrospun adsorbents outperform monolith and packed-bed resins in the oligo-dT affinity capture of therapeutic mRNA in dynamic binding capacities while showing comparable recovery and impurity removal regardless of mRNA chain length [28]. Additionally, affinity capture using electrospun adsorbents has been shown in the purification of AAV5 viral vectors using AVB ligand [29]. In this study, capsids were captured from clarified feed with high host cell protein and DNA removal. A series of residence times showed that there is time-dependent adsorption kinetics for AAV vectors. Furthermore, it was found that increased residence times and overloading the column can also negatively affect recovery of vectors. Both findings further highlight the advantages of using electrospun adsorbents in rapid cycling mode.

In ion-exchange applications, studies have focused on the purification of viral vectors to take advantage of the reduced steric exclusion from the structure of electrospun adsorbents. In Turnbull et al. [30]., it was shown that adenovirus 5 particles, around 90 nm in size, can effectively adsorb on electrospun adsorbents, highlighting the minimal steric exclusion from the open-pore structure of the fibrous adsorbent. In the study, it was shown that at low residence times, adenovirus 5 infectivity can be retained through the purification while host cell proteins and other impurities are removed [30]. Similarly, in Ruscic et al. [31]., an anion exchanger electrospun adsorbent was shown to purify lentiviral vectors, around 100 nm in size, with low residence times while maintaining high recoveries. In Ruscic et al., an adsorption-time dependent deactivation of lentiviral vector infectivity was shown, which again highlights the electrospun adsorbent's advantages when used as rapid cycling media. It was found that this deactivation can be minimalised by reducing the adsorption time for lentivirus particles on the adsorbent. Finally, both papers also highlighted the importance of controlling ligand density for anion exchange media to minimize viral vector deactivation.

In further studies, non-cellulosic polymer backbones were also investigated. In Ng et al., series of cation exchanged polyacrylonitrile electrospun adsorbents were analysed for their ability to purify C-phycocyanin from allophycocyanin and other contaminating species [32]. Ng et al.'s findings are consistent with other electrospun membrane findings in flowrate independence of breakthrough curves of binding of target species and contaminants. Furthermore, this study confirmed that modifying the polymer backbone with added chitosan polymer in the electrospinning solution modifies nanofiber structure and increases c-phycocyanin capacity.

Competing membrane technologies have been applied in lentivirus and adenovirus purification [33,34] and in adeno-associated virus polishing steps to separate full from empty capsids [35]. Furthermore, ion-exchange membranes and monolithic adsorbents have been shown to be able to purify plasmid DNA feeds and even separate isoforms of the plasmid, while there has been no published study on the plasmid DNA purification using electrospun adsorbents to date [36,37].

Even though there are various applications of electrospun adsorbents and other convective media in bioprocessing as highlighted above, most of the current literature focuses on proof of concept and showcasing applications. There is a lack of published data on rational design of adsorbent fiber structure to improve capacities and performance in a downstream processing application. To address this, the goal was set out to rationally design the fiber structure of the adsorbents and to understand the underlying performance in downstream processing. In this paper, electrospun adsorbents are characterised with a wide range of analytical techniques to be able to draw a connection between downstream processing performance and physical characteristics. This study will help rational fiber adsorbent design to improve downstream processing capabilities of the electrospun adsorbents.

2. Materials and methods

2.1. Electrospinning

The method for the manufacture of the cellulose electrospun adsorbents in this paper follows the method outlined in the Patent WO2015052465A1 [17]. The electrospinner used for the experiments was a Nanospider NS 1S500U lab-scale electrospinner manufactured by Elmarco (Liberec, Czech Republic). In order to generate the fibers, a solution of 6, 8 and 10 % (w/w) cellulose acetate (CA) solution was

mixed in 3:1 ratio of acetic acid and ethanol (CAS Number: 64–19–7 and CAS Number: 64–17–5 respectively). An additional 5 % polyethylene oxide aqueous solution was added at 1.2 % (w/w) of the overall polymer solution. Cellulose acetate (CA) (Mn~ 50,000, CAS Number: 9004–35–7), acetic acid (CAS Number: 64–19–7), ethanol (CAS Number: 64–17–5) were all acquired from Sigma Aldrich.

2.2. Lamination

The lamination of the electrospun sheets was done on a Reliant Powerbond 100 manufactured by Reliant Machinery (Luton, UK). Single layer sheets were laminated together one on top of the other until the desired adsorbent mass per unit surface area was met (ranging from 8 to 10 layers, depending on prototype). A temperature ramp was made using the heating modules from 170 °C to 185 °C and the laminating pressure was varied between 1, 2, and 5 bar to achieve the different compressions. Roller gap was maintained at 0 mm for the process. This method for electrospun adsorbent lamination is also outlined in Patent WO2015052465A1 [17].

2.3. Chemical functionalisation

The method for the chemical functionalisation of the cellulose adsorbents in this paper follows the method outlined in the European Patent EP3187260B1 [38]. To deacylitate the CA into regenerated cellulose (RC), samples were held in 0.5 M NaOH solution with 2:1 water to ethanol ratio for 6 h. Samples were then washed in DI water until neutral pH was achieved again. RC was functionalised with the quaternary amine (Q) by submerging the adsorbents in a 0.5 M NaOH mixed with either 100 ml or 300 ml Glycidyltrimethylammonium chloride (Sigma Aldrich, CAS-No: 3033–77–0) to achieve the desired high or low ligand density.

2.4. Thickness and porosity

To measure the thickness of the adsorbent sheet a Mitutoyo ABSOLUTE (Tokyo, Japan) measuring system was used. A total of 3 discs was taken from each sheet and each disc was measured five times at different positions. Each measurement was recorded and averaged. Once the thickness was measured, the samples were also heated to 110 °C and weighed in order to determine their dry mass. Then the dry mass and thickness was used to estimate the porosity using the following formula:

$$\varepsilon = \frac{\frac{Mass_{Sheet}}{Volume_{Sheet}} + \rho_{Cellulose}}{\rho_{Air} - \rho_{Cellulose}} \quad (1)$$

Where $Mass_{Sheet}$ and $Volume_{Sheet}$ are the measured mass and volume of the sheet, respectively, ε is the porosity of the adsorbent, ρ_{air} is the density of air (which is used as 1.20 kg m^{-3}) and $\rho_{cellulose}$ is the skeletal density of cellulose (which is used as 1322 kg m^{-3} determined from Helium Pycnometer, data not shown).

2.5. Capillary flow porometry

To estimate the apparent pore size, a Porolux 100 porometer w by Porometer (Nazareth, Belgium) was used. 25 mm discs were cut and immersed in Porefil™ wetting fluid with known surface tension (16.05 ± 0.06 nM/s at 23 °C). These samples were then loaded into the porometer machine and were analysed between 0.4 and 3.0 bar while measuring the flow rate.

2.6. Scanning electron microscopy (SEM)

Samples were gold-coated by a Quorum Q150R S gold coater (Laughton, UK) for 5 min. After the gold coating, five images of each sample were taken using a PhemonPro scanning electron microscope (Thermo Fisher Scientific, UK). Next, these images were viewed and analysed using the FiberMetric software from Phenom Software.

2.7. Titration

Ligand density was determined by using the Mohr Method [39]. Adsorbents were first washed with a serial dilution of hydrochloric acid (0.1 M, 0.01 M, 0.001 M). Samples were then dried and weighed to determine their dry mass. 1 ml of Potassium chromate 5 % solution (VWR, CAS-No: 7789–00–6) was added to the sample and was titrated using 0.1 N Silver Nitrate (VWR, CAS-No: 7761–88–8) until a colour change was observed from bright yellow to dark brown.

2.8. Static binding capacity

Static binding capacity was determined by punching 2.5 mm diameter discs, using a biopsy hole puncher, from the adsorbent sheet and washed three times in 20 mM Tris buffer at pH 8. Sample were then placed in 96 well plates and submerged in 150 µL of 20 mM Tris binding buffer at pH 8 and a known dilution of protein or plasmid DNA was added. The tray was incubated overnight on an orbital shaker at 100 rpm and the protein concentration in the well was analysed by NanoDrop™ OneC UV–Vis spectrophotometer (Thermo Fisher Scientific, UK). Data was then fitted using partial least squares with the Langmuir isotherm to determine maximum binding capacity (Q_{max}).

Three model biologics were chosen for the adsorption as shown in Table 1. The two proteins were bovine albumin serum (BSA) (CAS Number: 9048–46–8) and thyroglobulin (CAS Number: 9010–34–8) and were ordered from Sigma Aldrich. The plasmid deoxyribonucleic acid (pDNA) was a gift from Didier Trono (Addgene plasmid # 12,251) and originally serves as a packaging plasmid containing coding for the Gag and Pol packaging proteins for lentivirus production [40]. The pDNA was grown in *Escherichia coli* and purified using a PureLink HiPure Expi Plasmid Megaprep Kit from Thermo-Fisher Scientific

2.9. Nitrogen isotherm surface area

The Brunauer–Emmett–Teller (BET) surface area was determined using a full nitrogen adsorption and desorption isotherm on a Micromeritics TriStar II PLUS machine (Tewkesbury, UK). At least 0.5 gs of each prototype of RC sample was dried at 140 °C under vacuum for 30 min. Then samples were characterised for their nitrogen isotherms using the procedure recommended by the manufacturer of the equipment. Each prototype was measured for BET surface area in triplicates. The BET model was then fitted to the data in order to determine specific surface area.

Along determining Q_{max}, a theoretical monolayer capacity was also determined by calculating how much adsorbate could fit on the adsorbent using the BET surface area according to Eq. (2). In Eq. (2), to get the equilibrium binding capacity in mg/ml of membrane, the BET surface area in m^2/g was multiplied by the membrane density to get surface area of membrane per membrane volume. This surface area was then divided by the projected area covered by the adsorbate, assuming adsorbates to be spherical using the Stokes Radius. Additionally, a packing coefficient of 1.102 was used to account for the packing of circles in a plane [44].

Table 1
Summary of key features of the three chosen model biologics.

Name	Size (unit varies)	Stokes Radius (R_H) (nm)	Isoelectric Point	Shape
BSA	65 kDa	3.5 nm [41]	4.9 [42]	Globular
Thyroglobulin	670 kDa	8.6 nm [41]	4.5 [42]	Globular
pDNA	8995 base pairs	39 nm*	4.35 [43]	Super-coiled

*Measured by dynamic light scattering.

$$Equilibrium\ Capacity = \frac{BET\ surface\ area\ \times membrane\ density}{Packing\ coefficient\ \times Projected\ Area\ of\ Adsorbate} \quad (2)$$

2.10. Measuring pressure drop and calculating permeability

The permeability was determined on an ÄKTA pure™ (Cytiva, Uppsala). An empty sample holder was characterised for its pressure drop. After, a 25 mm disc was placed in the sample holder and pressure drop across the adsorbent holder was determined at 5, 10, 15, 20, and 25 ml min^{-1} flowrates. Each disc was tested three times and two discs of each prototype were used. The pressure drop from the sample holder was subtracted and a linear line of best fit was fitted. Using the Darcy equation, a permeability for each sheet was developed:

$$Q = -\frac{\kappa}{\mu L}\Delta P \quad (3)$$

Eq. (3) where Q is the volumetric flowrate, K is the permeability, μ is the dynamic viscosity, L is the thickness of the sheet and ΔP is the pressure drop along the sheet. All values in their SI units.

From Choong et al., a modified version of the semi-empirical Ergun equation for flow past nano-sized fibers was used to determine a pressure drop theoretically [45]:

$$\frac{\Delta P}{L} = 150\frac{(1-\varepsilon_B)^2 \nu \mu}{\varepsilon_B^3 d_s^2} + 1.75\frac{(1-\varepsilon_B)\nu^2 \rho}{\varepsilon_B^3 d_S} \quad (4)$$

Where ΔP/L is the pressure drop per unit thickness of adsorbent sheet, ε is the porosity of the bed (electrospun adsorbent sheet in this case), ν is the superficial velocity of the liquid, μ is the dynamic viscosity, ρ is the density of the fluid and d_s is the characteristic diameter of the fibers. All values in their SI units.

2.11. Dynamic binding capacity

The dynamic binding capacity (DBC) of the adsorbent prototypes for each of the proteins and plasmid DNA was determined by frontal analysis. A 25 mm disc was placed in sample holder and were connected to an ÄKTA pure™. Sample holders are purpose-built units made from polyether ether ketone (PEEK) polymer. The membrane was sandwiched between two metal frits with 50 μm pore size and sealed with a rubber O-ring. The sample holders with the metal frits were measured to have a hold-up volume of 1.1 ml. Each adsorbent had a unique height and individual adsorbent volumes are collected and summarized in the Supplementary Data section.

All flowrates were fixed at 15 ml/min for the DBC measurements. The column was equilibrated with 20 mM Tris buffer at pH 8 for 10 ml of buffer. Then solution of 0.5 mg/ml of BSA or thyroglobulin and 0.1 mg/ml of the pDNA was loaded onto the column until 10 % breakthrough was reached. A 1.0 M NaCl solution was applied to elute the adsorbed protein. The DBC (mg/mL adsorbent) at 10 % breakthrough was calculated from a simplified equation neglecting the unbound material under the curve up to 10 % breakthrough:

$$DBC = \frac{V\ \times\ c_0}{V_{adsorbent}} \quad (5)$$

Where C_0 and V is the initial adsorbate concentration and loading volume at 10 % breakthrough, respectively; V_{sheet} is the volume of adsorbent sheet.

2.12. X-ray computed tomography (CT) scanning

Regenerated cellulose samples were laser cut to 15.0 mm x 0.5 mm sizes while preserving the thickness. These samples were then mounted to a metal pin using epoxy glue from one end of the strip so the top part would be not touched by epoxy. Once the epoxy cured, the samples were mounted into the sample holder and scanned. During the scanning process, an area of the adsorbent was selected that did not come into contact with the epoxy and was not shielded by the metal pin. For scanning, a 0.5 mm x 0.5 mm x 0.5 mm field of view was selected in order to ensure scanning through the full thickness of the adsorbent.

A ZEISS Xradia Versa 620 (Pleasanton, USA) was used to scan the electrospun adsorbent. A primary accelerating voltage of 40 keV was applied with a 3 W power rating in each case over 1601 projections, achieving a pixel size of 400 nm using a 20X lens at a 15 s exposure. An enhanced pixel size of 200 nm of an internal volume was achieved by applying an extended 120 s exposure time, otherwise using identical settings [46]. Digital volumes were reconstructed using Avizo software (Thermo Fisher, USA) into TXM files that were cropped to produce 3D TIFF files. An additional pixel-by-pixel analysis was applied using Matlab software (Mathworks, USA).

3. Results and discussion

3.1. Fabrication of electrospun adsorbents

As shown on Fig. 1, a four-step process is used to generate the electrospun adsorbent prototypes. The first step is the electrospinning process where the submicron size cellulose acetate fibers are formed. At this stage of the process, the critical properties are the fiber diameters which subsequently affect the total surface area of the fibers within the adsorbent. Fig. 2A shows the average fiber diameter of the prototypes. It can be seen that the lamination has no measurable effect on the mean fiber diameter. This was measured by the SEM imaging technique which showed no change in geometry or diameter on individual fibers in the structure of the adsorbent. However, changing the polymer concentration in the electrospinning process did have a measurable effect on the fiber diameter. Fig. 2A shows that the nine prototypes can be broken into the three clusters of similar mean fiber diameters. Through increasing the polymer concentration, the fiber diameter of the adsorbent was increased by 50 %. These clusters share the same polymer concentration in the electrospinning process.

In the second step of the process, lamination applies heat and pressure in order to give mechanical strength to the electrospun adsorbents [16]. However, this treatment also has an effect on the pore structure and porosity of the adsorbent. The three conditions tested (High, Medium, and Low) gave rise to three different porosities. Fig. 2C and 2D show that the lamination does greatly affect the apparent mean pore size measured by the capillary flow porometry and the porosity of the electrospun sheets as measured by density of the membrane. These measurements are orthogonal measurements as capillary flow porometry relies on a gas flow relationship through the adsorbent while porosity measurements rely on mass, volume, and skeletal density of cellulose to estimate the porosity. By increasing the laminating pressure from 1 to 5 bar, the porosity can be effectively reduced by 50 % on any of the adsorbent prototypes while apparent mean pore size can be reduced by 40 %.

Both of these measurements show that the pore structure and porosity can be independently manipulated by the lamination regardless of the electrospinning conditions from the previous step. In Fig. 2B, as expected, 50 % of lower diameter prototypes yield 75 % higher surface area per unit gram of electrospun adsorbent. Furthermore, at low and medium laminating pressures the electrospun adsorbents retain their surface area. However, Fig. 2B also shows that with high laminating pressures, the surface area begins to decrease by up to 40 %. This phenomena is most likely, due to pore closure and fiber fusion thus blocking some of the surface area of the fibers. To obtain the BET surface area, full nitrogen adsorption and desorption were run. On the isotherm, no hysteresis was observed and therefore, it is assumed that the microporosity of the adsorbent is negligible.

Fig. 3A shows the SEM images of the matrix of cellulose adsorbent after regeneration. On the SEM images, a wide range of fiber sizes can be

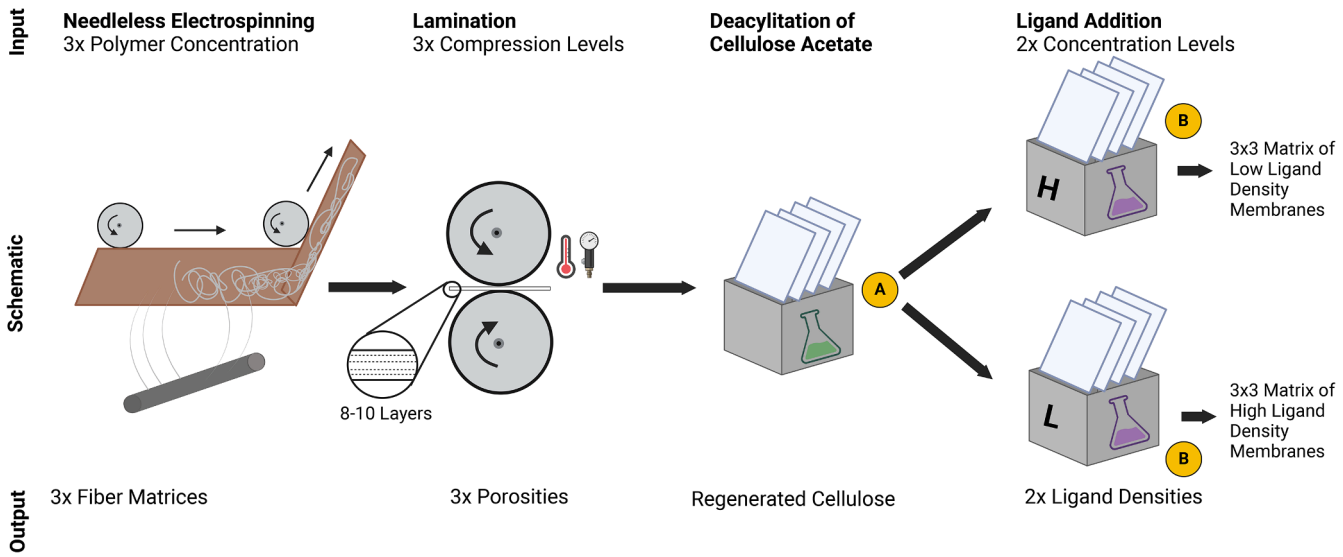

Fig. 1. Flow diagram showing the process of fabrication for the quaternary amine cellulose electrospun adsorbents.

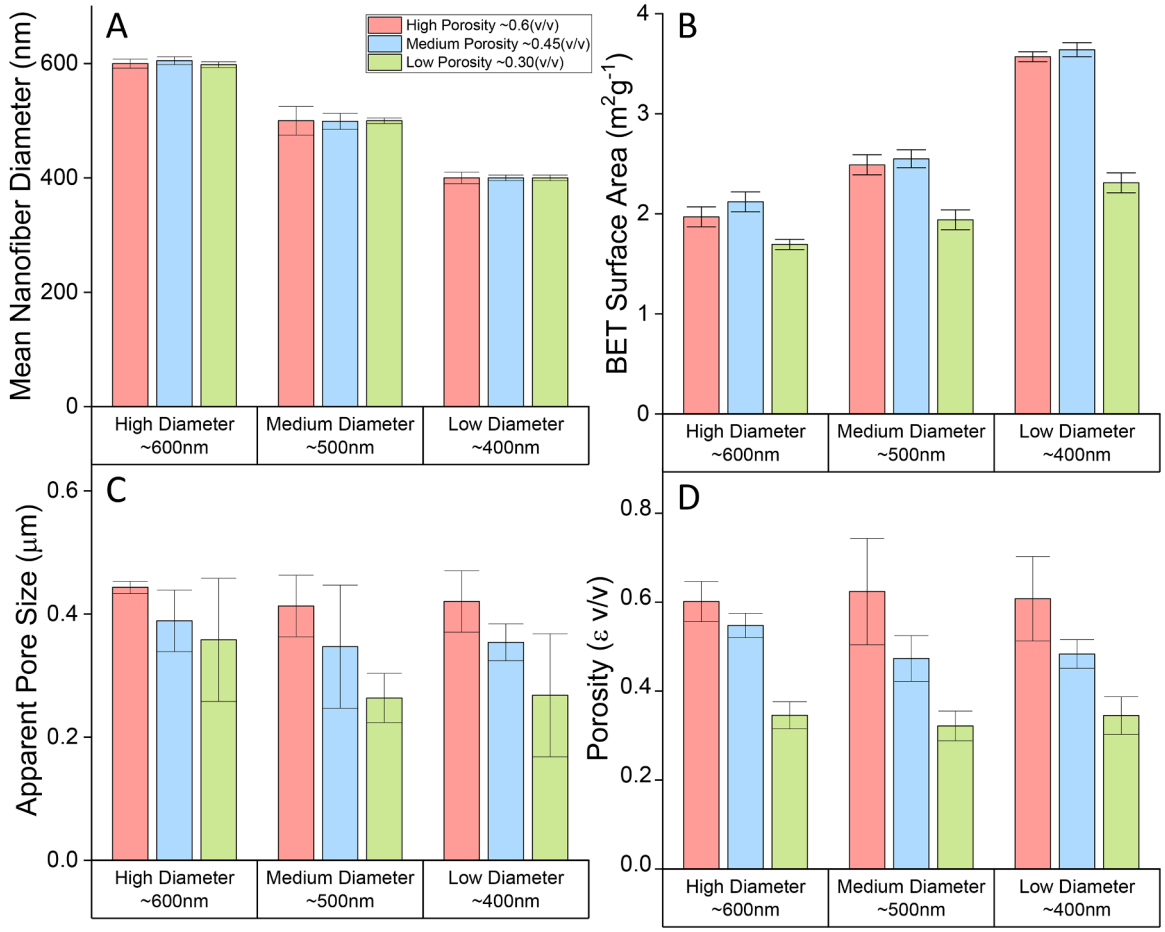

Fig. 2. Graphs showing the key physical characteristics of the nine prototype electrospun adsorbents after deacylitation. (A) mean fiber diameter measured by SEM image analysis. (B) BET surface area of the electrospun adsorbents measured by nitrogen adsorption. (C) apparent mean pore size of the electrospun adsorbents measured by capillary flow porometry. (D) porosity of the electrospun adsorbents as measured by the composite densities. Error bars show standard deviation in triplicate repeats of each measurement with the exception of (A), where five images were analysed.

seen present in a single electrospun sheet, as shown in the histograms in Fig. 3B. Qualitatively, one can see that the fibers within the sheet become more dense as the porosity decreases. However, computational analysis of this porosity did not show meaningful results as field of view of SEM images is too low to draw conclusions for the macroscopic porosity of the adsorbent. A further observation from the SEM images

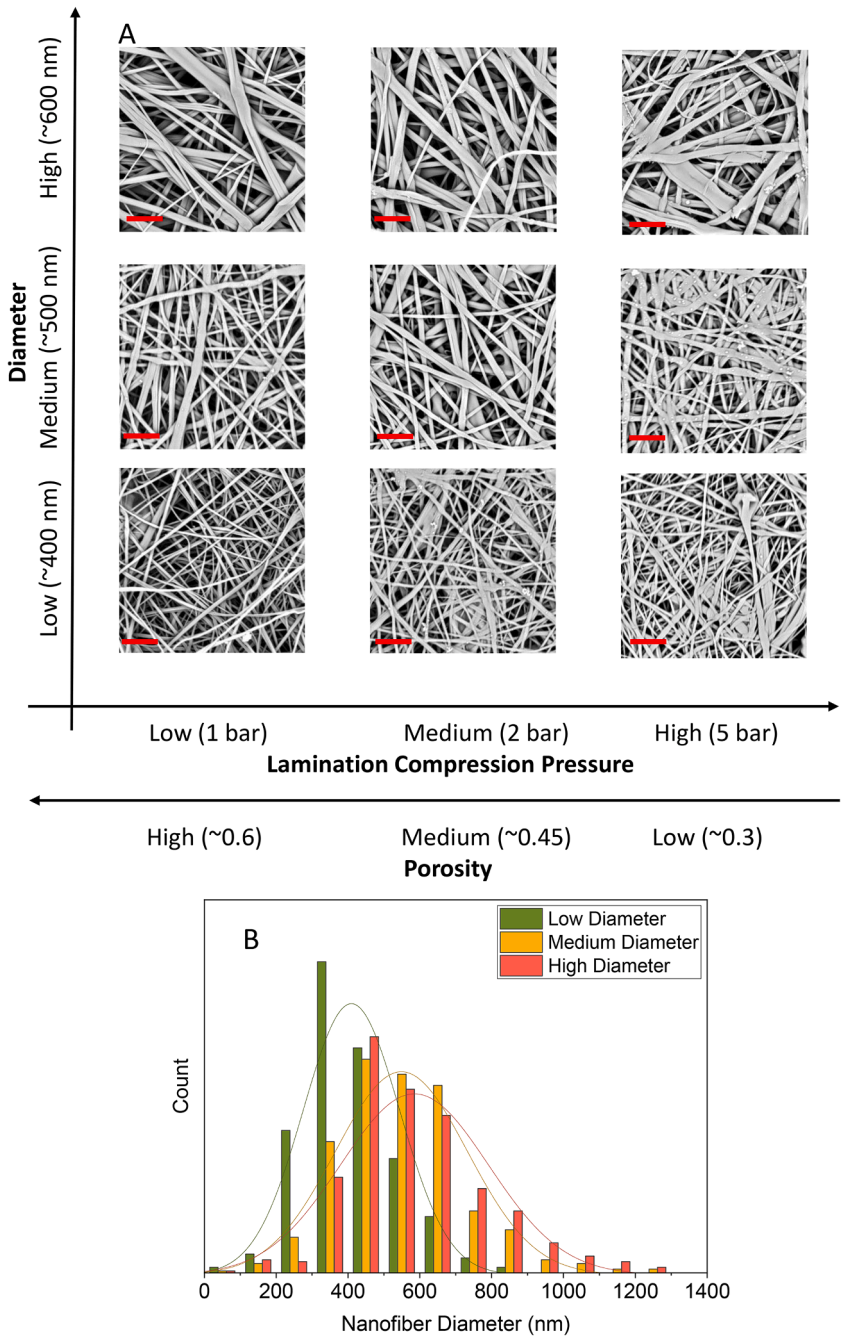

Fig. 3. (A) SEM images of the matrix of electrospun adsorbent structure after the chemical regeneration of cellulose. Images are taken at 10,000x magnification and scale bar shows 5 μm. (B) fiber size distribution of three subgroups of adsorbent membranes. Data collected using Phenom Pro fiber analysis software on 5 SEM scans at 10,000x magnification from each population.

was the wide range of fiber diameters that are present in any given adsorbent sheet. In each electrospun adsorbent sheet, there is a wide range of fiber diameters present as shown on Fig. 3B. This is in agreement with published results in other electrospinning processes and is widely accepted as a result of electrospinning's random Taylor cone formation phenomena. In Fig. 4, the 3D dimensional rendition of the CT scan data is presented in the same matrix format as Fig. 3. On this figure, a difference in fiber quality can be observed between electrospun adsorbent prototypes. The low diameter prototypes exhibited significantly more non-fibrous areas than the high diameter prototypes. Low diameter prototypes were fabricated through lowering the polymer content of the electrospinning solution and at lower viscosities, electrospinning can transition to electrospraying, thus forming more droplet-like structures. Determining the porosity computationally was also trialled, however, due to limited resolution of the CT scans, not all the fibers are picked in the scans. Therefore, absolute quantification of values including porosity and pore size were not considered representative at this resolution.

As discussed, the design space expands beyond that reported by Hardick et al. [20], notably by incorporating a lamination step in the synthesis of electrospun adsorbents. This step controls compression and porosity, significantly impacting the adsorption performance for biological products. Additionally, we provide robust measurements of physical properties, such as surface area.

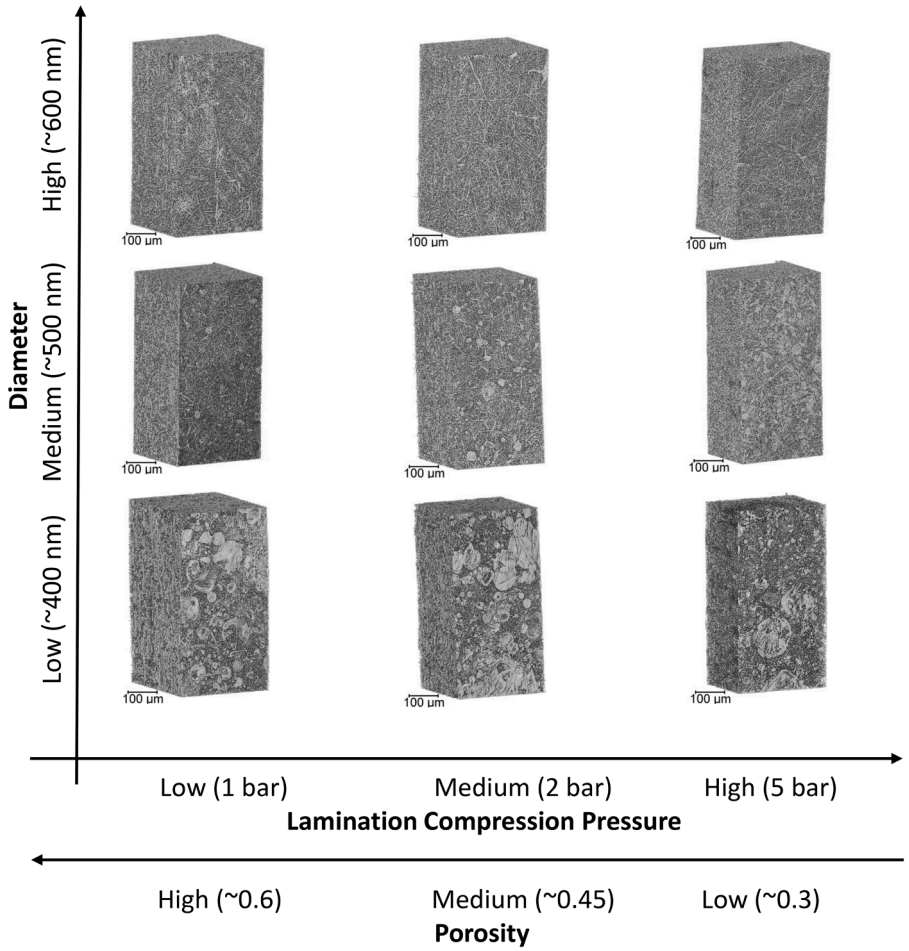

Fig. 4. X-ray CT scan of matrix of electrospun adsorbent structure after the chemical regeneration of cellulose. Regenerated cellulose samples were laser cut into size and attached to a pin using epoxy. Mounted samples were scanned in a ZEISS Xradia Versa 620 for 8 h with 15 second exposure time per projection with 1601 projections.

3.2. *Functionalisation of the electrospun adsorbent prototypes*

The cellulose acetate adsorbents were functionalised in a two-step reaction. First the adsorbents were deacylated to cellulose. This reaction was taken to completion as verified by Fourier-Transform Infrared Spectroscopy. Then the quaternary amine groups were immobilized onto the exposed hydroxyl groups in the final step of the process, as shown on Fig. 1. Two different ligand densities were chosen: one designated as high and one as low. It was found that the nine electrospun adsorbent prototypes would get a similar ligand density in the two

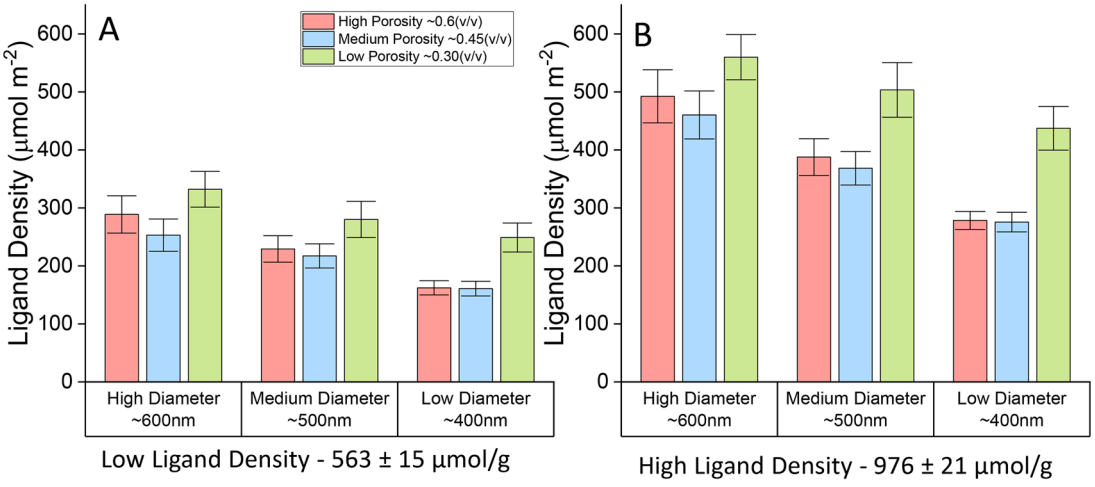

Fig. 5. Ligand densities measured by colorimetric ligand titration using the Mohr method after chemical functionalisation. Two 45 mm discs from each batch were measured for dry mass and titrated until a colour change was observed. Ligand densities of the electrospun adsorbents are expressed as moles of ligands per unit surface area for low ligand (A) and high ligand density (B) prototypes respectively. These were obtained by dividing the titration results by the BET values.

groups regardless of compression or fiber diameters. For the low ligand density, an average of 563 ± 15 μmol/g were obtained across the nine prototypes. For the high ligand density, an average of 976 ± 21 μmol/g was measured using ligand titration. Although the prototypes all come out to have similar measured ligand densities, they have different surface areas, Fig. 5A and 5B show the ligand densities per unit surface area. For higher surface area prototypes, ligand densities are lower as the charged groups get distributed over a larger area. This pattern holds true for most prototypes, except the high compression material which loses BET surface area during fabrication. Since biologics experience the charge on the surface of the adsorbent, charge densities normalized for surface area are expected to be a more representative measurement when thinking of adsorption. However, in this study, there was no observable effect of binding capacities as ligand density per unit surface area changes. This could be a result of high measurement error in binding capacity studies.

3.3. Determining the permeability of the electrospun adsorbent prototypes

Figure ˆA shows the raw data for runs on different electrospun adsorbents prototypes. As expected, low porosity electrospun adsorbents have a higher pressure drop across the 8–10 layer adsorbent sheets than more porous adsorbent prototypes. Fig. 6B shows the results for all nine prototypes plotted against the semi-empirical modified Ergun equation fitted for fibrous materials (as shown on Eq. 4). The correlation fits the data reasonably well, however, there are some data points that are still more than a factor of 10 underpredicted by the correlation. One of the drawbacks of this correlation is the use of physical parameters in dry conditions. There is currently a lack of analytical equipment to characterise electrospun membranes in wet conditions. Therefore, it is challenging to estimate porosity and fiber diameters in wet conditions for use in either mechanistic or empirical models. From the data, it can be concluded that lower compression and higher diameter prototypes yield more favourable permeability which is confirmed by the semi-empirical model and the empirical measurements. Fiber diameter is affecting the permeability to a smaller extent than compression of the adsorbent. This was confirmed as by decreasing the porosity by 50 %, the permeability decreased on average by a factor of 8 (ranging from 7 to 11) on the three prototype fiber structures. On the other hand, increasing the fiber diameter by 50 % only decreased permeability by a factor of 5 (ranging from 2 to 7).

3.4. Determining the static and dynamic binding of the electrospun adsorbent prototypes

Looking at the equilibrium adsorption behaviour of the adsorbent prototypes, we can see that both compression and fiber structure have effects on binding. In Fig. 7, the matrix of electrospun adsorbents prototypes can be seen and the raw data for the determination of the isotherm and Q_{max} of the prototypes is shown. All measurements are expressed as mg/ml of adsorbent as this is currently the most widely applied and therefore most easy to compare to values from literature [4, 34]. However, mg/ml of binding capacity does not account for varying porosities in the adsorbent structure. The general trend that we observed is that lower diameter prototypes have higher adsorption than higher diameter prototypes. A possible explanation for not seeing larger increases in the binding capacity across different fiber diameters can be the defects observed in the CT scans in Fig. 3. Qualitatively, an increase of non-fibrous areas can also be seen as the electrospinning process uses lower cellulose acetate content and lower viscosity solutions. The measured equilibrium binding capacity values are in line with values from literature measuring lysozyme maximum binding capacity in Dods. et al. at 13.0 mg/ml on similar electrospun adsorbent type [16]. On the other hand, medium porosity seems to have the highest adsorption. This correlates with previous findings that surface area is reduced at high lamination pressures.

On Fig. 8A, 8B, and 8C, a sample bind and elute chromatogram of BSA, thyroglobulin and pDNA, respectively, can be observed. Both BSA and thyroglobulin were high purity adsorbents with expected single peak elution. The adsorbent holder in this study was optimised for measuring breakthrough curves. It was not optimised for low elution volumes due to its high hold-up volume as compared to the adsorbent volume, however, the chromatograms shows that the system could concentrate the protein solution. The chromatograms for the pDNA separation show that the elution profile is not a single peak. This is most likely caused by heterogeneity of the pDNA isoforms and other contaminating species.

Fig. 8D and 8E show the relationship between dynamic and static binding capacities. It was found that the ratio of dynamic to static binding capacity is high as expected for electrospun adsorbents [16].

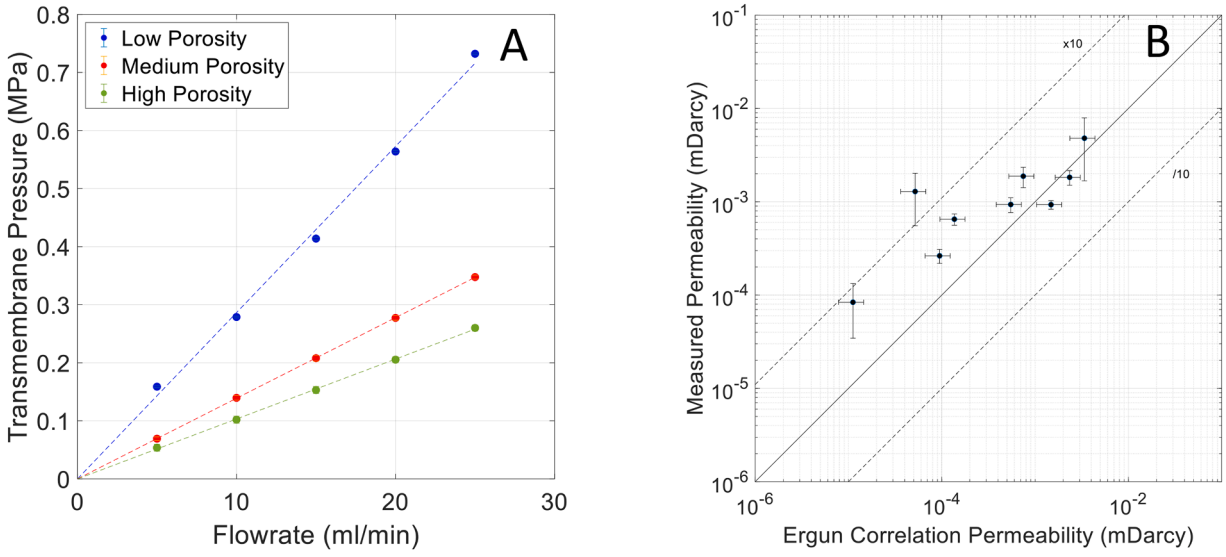

Fig. 6. (A) shows the raw data from medium fiber diameter prototypes of the pressure-flow relationship on the electrospun adsorbents. Error bars show standard deviation on the six taken measurements. (B) shows the permeability of the adsorbent sheet compared with the theoretical permeability obtained from the modified Ergun equation. A single 25 mm disc from each of the prototype was cut out and inserted into a sample holder designed for electrospun adsorbent testing. Sample holder was attached to an ÄKTA pure™, and pressure drop across membrane was measured within the 5 ml/min to 25 ml/min range.

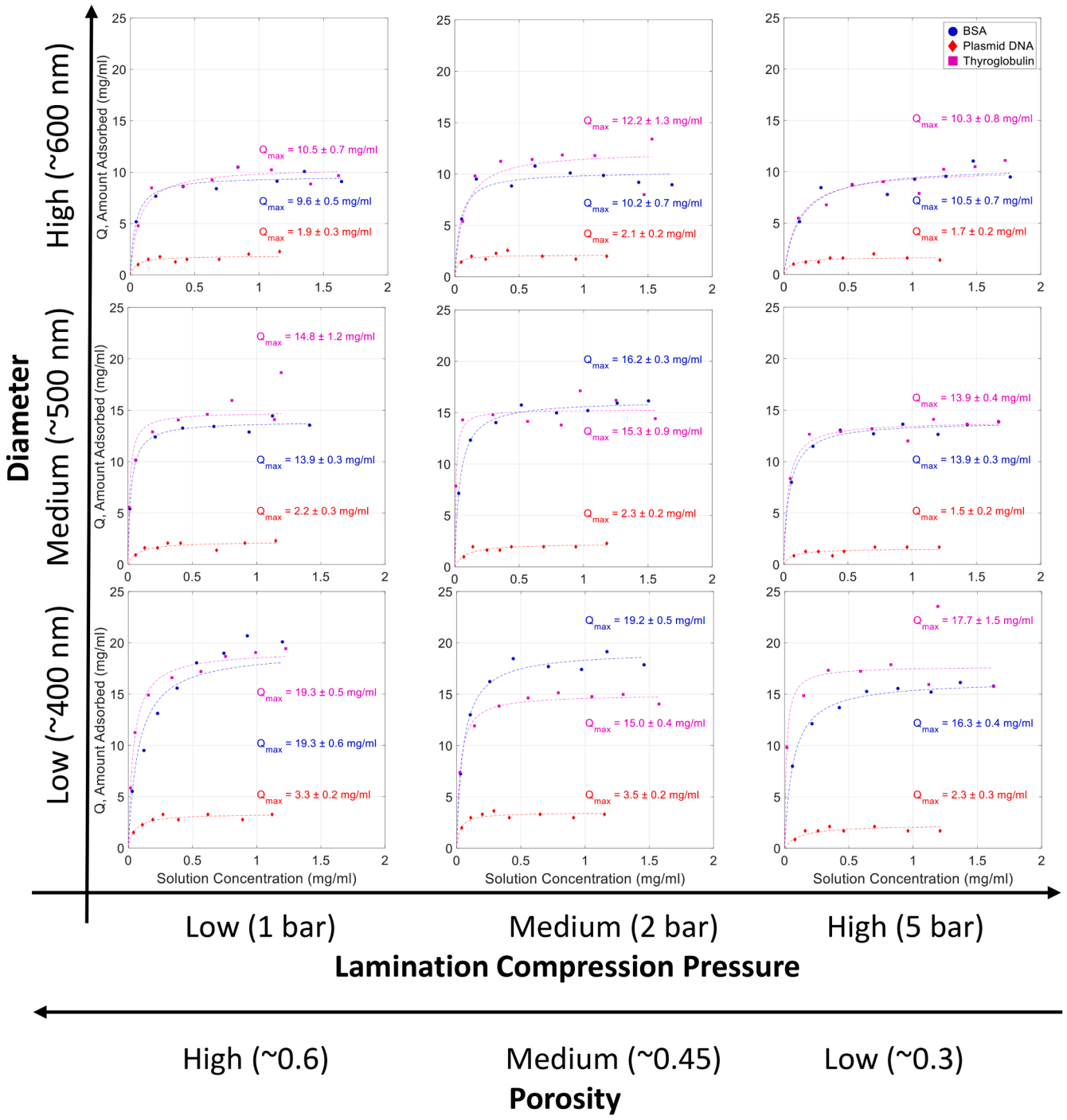

Fig. 7. Raw static adsorption data for the three adsorbates at low ligand density for the nine prototypes. The data was collected using a batch adsorption experiments in 200 μL well plates overnight. The data was then fitted using least squares fit method with a Langmuir Isotherm in order to extract the Q_{max} value for each prototype. Error shown on graphs is error from fitting on Q_{max} values. R^2 values all above 0.90. Blue circle – BSA, Red diamond – Plasmid DNA, Purple square – thyroglobulin.

However, it was found that at lower ligand density, there is a larger difference between static binding capacity and dynamic binding capacity with ratios ranging between 60 % to 91 % averaging at 71 %. On Fig. 8D, it can be seen that dynamic binding capacity is about 40 % lower across all prototypes than the static binding capacity. For higher ligand densities, not only do they offer higher binding capacities, their ratio of static and dynamic binding capacities is also higher ranging from 80 % to 98 % averaging at 89 %. Therefore, this data suggests that increasing ligand density can improve performance of these adsorbents in biologics separations. Dynamic binding capacities from these experiments are in line with values from literature where Hardick et al., showed 5 mg/ml binding capacity for BSA on comparable electrospun adsorbents [20]. It should also be noted that as the ligand densities are increased, one may run into recovery problems with biologics as elution might become a challenge. Therefore, it is not enough to just increase ligand density to maximize capacity, but also find a level where proteins can still be recovered during elution. At the ligand density levels used in this study, it was possible to recover the proteins with 1 M NaCl. However, for the pDNA the electrospun adsorbents could only be regenerated with 0.5 M NaOH wash. This finding is consistent with literature where quaternary

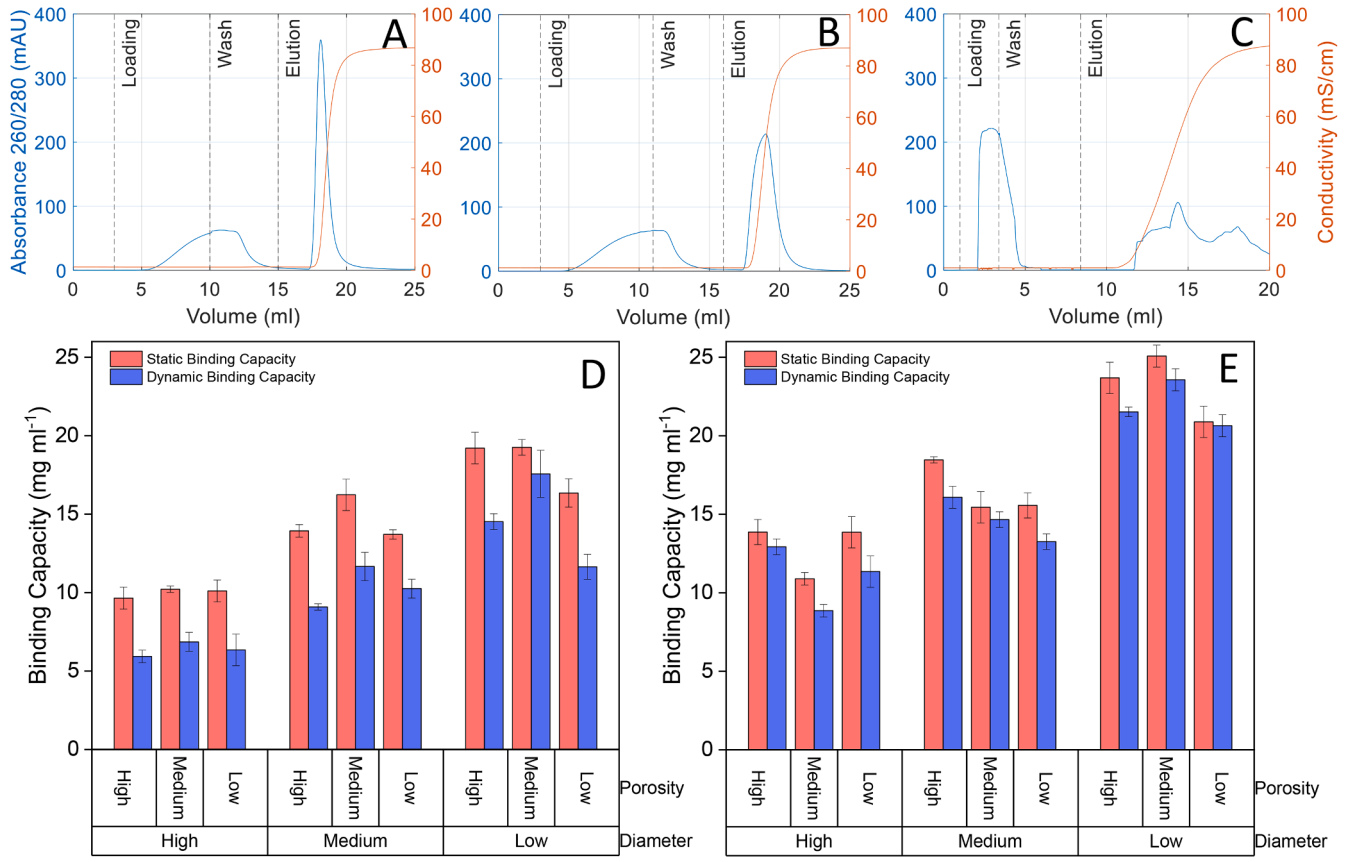

Fig. 8. (A,B), and (C) Representative bind and elute chromatograms for BSA, thyroglobulin and pDNA, respectively. Graphs showing the static and dynamic adsorption of BSA on the adsorbent prototypes. (D) and (E) show low and high ligand density results respectively. The dynamic binding capacity of the adsorbent prototypes for BSA was determined by frontal analysis. A 25 mm disc was placed in sample holder and were connected to an ÄKTA pure™. Loading flowrates were fixed at 15 ml/min for the DBC measurements and 0.5 mg/ml loading feed was used.

amine anion exchanger ligands have been shown to work in pDNA separation on other nucleic acid adsorptions. However, higher recoveries can be achieved using weak anion exchange resins (e.g. diethylaminoethyl, DEAE) when all other parameters were kept constant [47].

Fig. 9 shows the static adsorption of all 3 adsorbates on the surface of the electrospun adsorbent and plots it against the theoretical monolayer value based upon BET surface area from Eq. (2). At low ligand density, on Fig. 9A, static binding capacity is just below the expected monolayer adsorption and therefore, it is unlikely to be forming multilayer binding. From these results, it can be assumed that the fibers do not have inaccessible surface area based on BET surface area measurement for the proteins and even for the larger pDNA. Similarly, on the high ligand density static binding data on Fig. 9B, it is also close to the expected monolayer adsorption. In general, it can be concluded that the binding capacity of the electrospun adsorbents is highly driven by surface area.

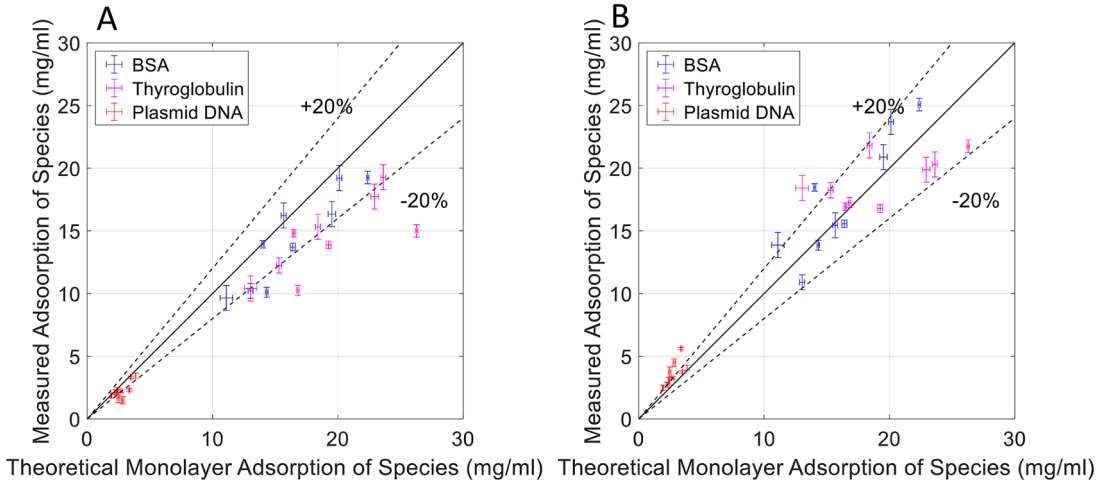

Fig. 9. Figures showing all Q_{max} values for all adsorbent prototypes with all adsorbates plotted against the theoretical monolayer adsorption using the BET surface area and the projected area of the adsorbate onto the fibers. (A) and (B) show low and high ligand density results respectively.

4. Conclusion

In this study, a series of electrospun prototypes were functionalised to create 18 strong anion exchange adsorbents. These materials were examined for their physical characteristics using porometry, CT imaging, SEM and BET surface area analysis. Utilizing data obtained from these assessments, theoretical models were proposed to explain the performance of electrospun adsorbents in a bioprocessing setting. The permeability of the adsorbents was measured and related to a semi-empirical model based on porosity and fiber diameter measurements. Also, a model for monolayer adsorption for proteins and plasmid DNA using the BET surface area was confirmed by static adsorption studies. Finally, a comparison between static and dynamic binding studies highlighted the advantage of electrospun adsorbents, which have convective mass transfer properties and exhibit limited steric hindrance, particularly beneficial for accommodating larger biologics.

To further improve the current models, a larger design space should be investigated with fibers diameters ranging from below 50 nm to above micron-size fibers. In addition, a further method to reduce fiber size distribution within adsorbents can also improve models which relate fiber diameter directly to static binding capacities. And there should be an ongoing development of physical characterisation methods for electrospun adsorbents in wet conditions to be able to better correlate fiber design to fiber performance in bioprocessing. A general observation is that proteins show higher binding in grams as they are higher density biologics when compared to plasmid DNA. Plasmid DNA is measured to have a large diameter through dynamic light scattering while their molar mass is comparable to a protein. The plasmid used in this study contains 8995 base pairs and has a molar mass estimated to be 333 kDa. This insight should be considered when comparing binding capacities of various biologics.

An area of interest in protein separation is further improving protein adsorption capacities using polymer grafting. Dextran and other polymer grafts have been shown to increase dynamic binding capacities in porous beaded resins [42]. Additionally, it has also been shown to improve capacities in affinity capture ligands on electrospun adsorbents with limited effect on permeability [48]. Polymer grafts could be further explored with ion-exchange ligands and whether the polymer graft has combinatorial effect with improved fiber morphology. Furthermore, the effect of polymer grafts on the steric hindrance of larger biologics can be investigated. Finally, to take advantage of the reduced steric hindrance of electrospun adsorbents and the rise of advanced therapy medicinal products, there is a need for an investigation into finding ideal electrospun adsorbent design for viral vectors and other nanoparticle materials above 50 nm size range while also balancing binding capacities and recoveries.

CRediT authorship contribution statement

Gyorgy Ovari: Writing – original draft, Investigation, Data curation. **Thomas F. Johnson:** Writing – review & editing, Software, Data curation. **Farzad Foroutan:** Writing – review & editing, Supervision. **Gunnar Malmquist:** Writing – review & editing, Supervision, Conceptualization. **Matthew Townsend:** Writing – review & editing, Supervision, Conceptualization. **Daniel G. Bracewell:** Writing – review & editing, Supervision, Funding acquisition, Conceptualization.

Declaration of competing interest

The authors declare the following financial interests/personal relationships which may be considered as potential competing interests:

Gyorgy Ovari reports financial support and equipment, drugs, or supplies were provided by Cytiva Stevenage. Thomas F. Johnson reports financial support was provided by Medical Research Council (MRC) Innovation Scholarship Grant. Thomas F. Johnson reports equipment, drugs, or supplies was provided by National Research Facility for Lab X-ray CT (NXCT). Gunnar Malmquist reports a relationship with Cytiva Sweden AB that includes: consulting or advisory and employment. Matthew Townsend reports a relationship with Cytiva that includes: employment. Farzad Foroutan reports a relationship with Cytiva that includes: employment. If there are other authors, they declare that they have no known competing financial interests or personal relationships that could have appeared to influence the work reported in this paper.

Data availability

The data that has been used is confidential.

Acknowledgements

This work was supported by EPSRC Centre for Doctoral Training in Bioprocess Engineering Leadership (Complex Biological Products Manufacture) (EP/S021868/1) and Cytiva. A grant from the National X-ray Computed Tomography (NXCT) was used to image adsorbent prototypes. The plasmid DNA used in this paper was a gift from Didier Trono. Thomas Johnson acknowledges funding from a Medical Research Council (MRC) Innovation Scholarship Grant MR/W004399/1 and EPSRC grant EP/T02593X/1 for accessing the National Research Facility for Lab X-ray CT (NXCT).

Supplementary materials

Supplementary material associated with this article can be found, in the online version, at doi:10.1016/j.chroma.2024.465268.

References

[1] A.C.A. Roque, A.S. Pina, A.M. Azevedo, R. Aires-Barros, A. Jungbauer, G. Di Profio, et al., Anything but conventional chromatography approaches in bioseparation, Biotechnol. J. 15 (8) (2020) 1–8.
[2] Sartorius. High throughput screening using membrane chromatography. 2015;1–4.
[3] Cytiva Global Life Sciences Solutions USA LLC. HiTrap fibro PrismA and HiScreen Fibro PrismA affinity chromatography product brochure. 2021;1–8. Available from: https://cdn.cytivalifesciences.com/api/public/content/digi-33339-pdf.
[4] MilliporeSigma. Natrix® Q Chromatography Membrane. 2020;2–3. Available from: https://www.merckmillipore.com/IE/en/product/Natrix-Q-Chromatography-Membrane,MM_NF-C197367.
[5] J. Thömmes, M.-R.. Kula, Membrane chromatography—An integrative concept in the downstream processing of proteins, Biotechnol Prog 11 (4) (1995) 357–367 [Internet][cited 2024 Mar 1]Available from, https://pubs.acs.org/sharingguidelines.
[6] M. Najafi, M.W. Frey, Electrospun nanofibers for chemical separation, Nanomaterials 10 (5) (2021) 982 [Internet]. 2020 May 21 [citedJan 25]Available from, https://www.mdpi.com/2079-4991/10/5/982.
[7] O. Hardick, B. Stevens, D.G. Bracewell, Nanofibre fabrication in a temperature and humidity controlled environment for improved fibre consistency, J. Mater. Sci. 46 (11) (2011) 3890–3898.
[8] M.S. Islam, B.C. Ang, A. Andriyana, A.M. Afifi, A review on fabrication of nanofibers via electrospinning and their applications, SN Appl Sci [Internet] 1 (10) (2019) 1–16, https://doi.org/10.1007/s42452-019-1288-4. Available from.
[9] T.G. Kim, H.J. Chung, T.G. Park, Macroporous and nanofibrous hyaluronic acid/collagen hybrid scaffold fabricated by concurrent electrospinning and deposition/leaching of salt particles, Acta Biomater. 4 (6) (2008) 1611–1619.
[10] E. DeSimone, T.B. Aigner, M. Humenik, G. Lang, T Scheibel, Aqueous electrospinning of recombinant spider silk proteins, Mater Sci Eng C [Internet] 106 (2020) 110145, https://doi.org/10.1016/j.msec.2019.110145. Available from.
[11] N. Radacsi, K.P. Giapis, G. Ovari, P. Szabó-Révész, R. Ambrus, Electrospun nanofiber-based niflumic acid capsules with superior physicochemical properties, J. Pharm. Biomed. Anal. 166 (2019) 371–378.
[12] A.F.C. Rengifo, N.M. Stefanes, J. Toigo, C. Mendes, D.F. Argenta, M.E.R. Dotto, et al., PEO-chitosan nanofibers containing carboxymethyl-hexanoyl chitosan/dodecyl sulfate nanoparticles loaded with pyrazoline for skin cancer treatment, Eur Polym J [Internet] 119 (2019) 335–343, https://doi.org/10.1016/j.eurpolymj.2019.08.001. Available from.
[13] L. Cseri, F. Topuz, M.A. Abdulhamid, A. Alammar, P.M. Budd, G. Szekely, Electrospun adsorptive nanofibrous membranes from ion exchange polymers to snare textile dyes from wastewater, Adv Mater Technol (2021) 2000955 [Internet] Jan 27 [cited 2021 Jan 30]Available from, https://onlinelibrary.wiley.com/doi/10.1002/admt.202000955.

[14] Zhao R., Wang Y., Li X., Sun B., Wang C. Synthesis of β-cyclodextrin-based electrospun nanofiber membranes for highly efficient adsorption and separation of methylene blue. 2015 [cited 2020 Dec 7]; Available from: www.acsami.org.
[15] T. Yao, J. Song, Y. Gan, L. Qiao, K. Du, Preparation of cellulose-based chromatographic medium for biological separation: a review, J. Chromatogr. A 1677 (2022) 463297.
[16] S.R. Dods, O. Hardick, B. Stevens, D.G. Bracewell, Fabricating electrospun cellulose nanofibre adsorbents for ion-exchange chromatography, J. Chromatogr. A 1376 (2015) 74–83, https://doi.org/10.1016/j.chroma.2014.12.010 [Internet]Available from:.
[17] O. Hardick, Bracewell daniel gilbert, dods stewart. Chromatography medium [Internet], Espacenet; WO2015052465A1, 2014 [cited 2024 Mar 1]. Available from, https://worldwide.espacenet.com/patent/search/family/049486506/publication/WO2015052465A1?q=WO2015052465A1.
[18] Z. Ma, S. Ramakrishna, Electrospun regenerated cellulose nanofiber affinity membrane functionalized with protein A/G for IgG purification, J. Memb. Sci 319 (1–2) (2008) 23–28.
[19] L. Zhang, T.J. Menkhaus, H. Fong, Fabrication and bioseparation studies of adsorptive membranes/felts made from electrospun cellulose acetate nanofibers, J. Memb. Sci 319 (1–2) (2008) 176–184.
[20] O. Hardick, S. Dods, B. Stevens, D.G. Bracewell, Nanofiber adsorbents for high productivity downstream processing, Biotechnol. Bioeng. 110 (4) (2013) 1119–1128.
[21] S.M. Lemma, C. Boi, R.G. Carbonell, Nonwoven ion-exchange membranes with high protein binding capacity for bioseparations, Membranes (Basel) 11 (3) (2021).
[22] H. Varadaraju, S. Schneiderman, L. Zhang, H. Fong, T.J. Menkhaus, Process and economic evaluation for monoclonal antibody purification using a membrane-only process, Biotechnol Prog 27 (5) (2011) 1297–1305 [Internet]Sep 1 [cited 2021 Sep 3]Available from, https://aiche-onlinelibrary-wiley-com.libproxy.ucl.ac.uk/doi/full/10.1002/btpr.639.
[23] R. Jacquemart, M. Vandersluis, M. Zhao, K. Sukhija, N. Sidhu, J. Stout, A single-use strategy to enable manufacturing of affordable biologics, Comput. Struct. Biotechnol. J. 14 (2016) 309 [Internet][cited 2024 Mar 1]Available from: /pmc/articles/PMC4990569/.
[24] O. Hardick, S. Dods, B. Stevens, D.G. Bracewell, Nanofiber adsorbents for high productivity continuous downstream processing, J. Biotechnol. [Internet] 213 (2015) 74–82, https://doi.org/10.1016/j.jbiotec.2015.01.031. Available from.
[25] S. Rajesh, C. Crandall, S. Schneiderman, T.J. Menkhaus, Cellulose- graft-polyethyleneamidoamine anion-exchange nanofiber membranes for simultaneous protein adsorption and virus filtration, ACS Appl. Nano. Mater 1 (7) (2018) 3321–3330. Jul 27.
[26] N. Gehrmann, A. Daxbacher, R. Hahn, Rapid purification of mAb using protein a membranes yielding high HCP clearance, J. Chromatogr. B 1232 (2024) 123989. Jan 1.
[27] S. Yang, R. Braczkowski, S.H. Chen, R. Busse, Y. Li, L. Fabri, et al., Scalability of Sartobind® rapid a membrane for high productivity monoclonal antibody capture, Membr 13 (2023) 815 [Internet]. Available from, https://www.mdpi.com/2077-0375/13/10/815/htm.
[28] E.A. Dewar, P. Guterstam, D. Holland, S. Lindman, P. Lundbäck, S. Brito dos Santos, et al., Improved mRNA affinity chromatography binding capacity and throughput using an oligo-dT immobilized electrospun polymer nanofiber adsorbent, J. Chromatogr. A 1717 (2024) 464670.
[29] S. Neto, J.P. Mendes, S.B.D. Santos, A. Solbrand, M.J.T. Carrondo, C. Peixoto, et al., Efficient adeno-associated virus serotype 5 capture with affinity functionalized nanofiber adsorbents, Front Bioeng Biotechnol 11 (2023) 1183974.
[30] J. Turnbull, B. Wright, N.K. Green, R. Tarrant, I. Roberts, O. Hardick, et al., Adenovirus 5 recovery using nanofiber ion-exchange adsorbents, Biotechnol. Bioeng. 116 (7) (2019) 1698–1709 [Internet]Jul 28 [cited 2020 Oct 15]Available from, https://onlinelibrary.wiley.com/doi/abs/10.1002/bit.26972.
[31] J. Ruscic, C. Perry, T. Mukhopadhyay, Y. Takeuchi, D.G. Bracewell, Lentiviral vector purification using nanofiber ion-exchange chromatography, Mol Ther - Methods Clin Dev 15 (2019) 52–62, https://doi.org/10.1016/j.omtm.2019.08.007 [Internet]Dec 13 [cited 2021 Jan 26]Available from.
[32] Ng I.-S., Tang M.S.Y., Loke Show P., Chiou Z.-M., Tsai J.-C., Chang Y.-K. Enhancement of C-phycocyanin purity using negative chromatography with chitosan-modified nanofiber membrane. 2019 [cited 2024 Jun 28]; Available from: https://doi.org/10.1016/j.ijbiomac.2019.03.235.
[33] A.S. Moreira, T.Q. Faria, J.G. Oliveira, A. Kavara, M. Schofield, T. Sanderson, et al., Enhancing the purification of Lentiviral vectors for clinical applications, Sep. Purif. Technol. 274 (2021) 118598. Nov 1.
[34] K. Kawka, A.N. Wilton, E.J. Redmond, M.F.C. Medina, B.D. Lichty, R. Ghosh, et al., Comparison of the performance of anion exchange membrane materials for adenovirus purification using laterally-fed membrane chromatography, Biochem. Eng. J. 182 (2022) 108417. May 1.
[35] A.L. Hejmowski, K. Boenning, J. Huato, A. Kavara, M. Schofield, Novel anion exchange membrane chromatography method for the separation of empty and full adeno-associated virus, Biotechnol J [Internet]. 17 (2) (2022) 2100219. Feb 1 [cited 2024 Mar 1]Available from, https://onlinelibrary.wiley.com/doi/full/10.1002/biot.202100219.
[36] Š. Kralj, Š.M. Kodermac, I. Bergoč, T. Kostelec, A. Podgornik, A. Štrancar, et al., Effect of plasmid DNA isoforms on preparative anion exchange chromatography, Electrophoresis [Internet] 44 (24) (2023) 1953–1966. Dec 1 [cited 2024 Mar 1] Available from, https://onlinelibrary.wiley.com/doi/full/10.1002/elps.202300035.
[37] M.A. Teeters, S.E. Conrardy, B.L. Thomas, T.W. Root, E.N. Lightfoot, Adsorptive membrane chromatography for purification of plasmid DNA, J. Chromatogr. A 989 (1) (2003) 165–173.
[38] HARDICK OLIVER, BRACEWELL DANIEL GILBERT, Dods stewart. functionalised chromatography medium [Internet], Espacenet, 2021. EP3187260B1[cited 2024 Mar 1]. Available from, https://worldwide.espacenet.com/patent/search/family/049486506/publication/EP3187260B1?q=pn%3DEP3187260B1.
[39] M. Sezey, P. Adun, Validation of mohr's titration method to determine salt in olive and olive brine, J. Turkish Chem. Soc. Sect. A Chem 6 (3) (2019) 329–334.
[40] T. Dull, R. Zufferey, M. Kelly, R.J. Mandel, M. Nguyen, D. Trono, et al., A third-generation lentivirus vector with a conditional packaging system, J. Virol. [Internet] 72 (11) (1998) 8463–8471. Nov 1 [cited 2024 Mar 1]Available from, https://pubmed.ncbi.nlm.nih.gov/9765382/.
[41] Verde V La, Dominici P, A Astegno, Determination of hydrodynamic radius of proteins by size exclusion chromatography, Bio Protoc 7 (8) (2017) [Internet]Apr 4 [cited 2023 Dec 14]Available from: /pmc/articles/PMC8410290/.
[42] Y. Yang, M. Yu, G. Ma, Z. Su, S. Zhang, Performance of agarose and gigaporous chromatographic media as function of pore-to-adsorbate size ratio over wide span from ovalbumin to virus like particles, J. Chromatogr. A 1638 (2021) 461879 [Internet]Feb [cited 2021 Jan 18]Available from, https://linkinghub.elsevier.com/retrieve/pii/S0021967321000030.
[43] G.V Sherbet, M.S. Lakshmi, F. Cajone, Isoelectric characteristics and the secondary structure of some nucleic acids, Biophys. Struct. Mech. 10 (3) (1983) 121–128 [Internet].Sep [cited 2023 Jun 22]Available from, https://link.springer.com/article/10.1007/BF00537554.
[44] Chang H.-C., Wang L.-C. A Simple Proof of Thue's Theorem on Circle Packing. [cited 2024 Jul 18]; Available from: http://en.wikipedia.org/wiki/Delaunay.
[45] LT (Simon) Choong, Z. Khan, G.C Rutledge, Permeability of electrospun fiber mats under hydraulic flow, J Memb Sci 451 (2014) 111–116.
[46] T.F. Johnson, F. Iacoviello, J.H. Welsh, P.R. Shearing, D.G. Bracewell, High-resolution imaging of depth filter structures using X-ray computed tomography, J. Mater. Sci. 56 (27) (2021) 15313–15326 [Internet]Sep 1 [cited 2024 Apr 23] Available from, https://link.springer.com/article/10.1007/s10853-021-06238-w.
[47] J. Stadler, R. Lemmens, T. Nyhammar, Plasmid DNA purification, J. Gene Med. 6 (SUPPL. 1) (2004). Feb.
[48] L. Huan, Q. Shi, Increasing immunoglobulin G adsorption in dextran-grafted protein A gels, Eng Life Sci [Internet]. 21 (6) (2021) 392–404. Jun 20 [cited 2021 Mar 28]Available from, https://onlinelibrary.wiley.com/doi/10.1002/elsc.202000097.